

Supplementary Information

## ***N*-Unsubstituted Thienoisindigos: Preparation, Molecular Packing and Ambipolar Organic Field-Effect Transistors**

*Dongho Yoo,<sup>a,\*</sup> Tsukasa Hasegawa,<sup>a</sup> Minoru Ashizawa,<sup>a,\*</sup> Tadashi Kawamoto,<sup>a</sup> Hiroyasu Masunaga,<sup>b</sup> Takaaki Hikima,<sup>c</sup> Hidetoshi Matsumoto<sup>a</sup> and Takehiko Mori<sup>a,\*</sup>*

Corresponding Authors

\*E-mail: yoo.d.aa@m.titech.ac.jp, ashizawa.m.aa@m.titech.ac.jp, and mori.t.ae@m.titech.ac.jp

<sup>a</sup> Department of Organic and polymeric Materials, Tokyo Institute of Technology, O-okayama 2-12-1, Meguro-ku, Tokyo 152-8552, Japan.

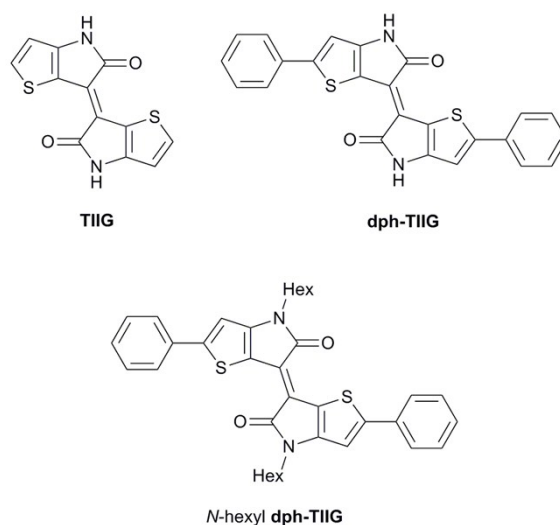
<sup>b</sup> Japan Synchrotron Radiation Research Institute (JASRI)/SPring-8, 1-1-1 Kouto, Sayo, Sayo 679-5198, Japan.

<sup>c</sup> RIKEN SPring-8 Center, 1-1-1 Kouto, Sayo, Sayo 679-5148, Japan.

## I. General

Commercially available materials were used as received. Anhydrous solvents (toluene and dichloromethane) were purchased from Wako Pure Chemical Industries. All reactions were conducted under argon atmosphere. For thin-layer chromatography (TLC) analysis, Merck pre-coated glass plates (TLC Silica gel 60 F254) were used. Silica gel used in chromatographic separations was obtained from Wako Pure Chemical Industries (Wako Silica Gel C-200 (spherical, neutral), 75–150  $\mu\text{m}$ ).  $^1\text{H}$  NMR (300 MHz) spectra were obtained with a JEOL JNM-AL300 spectrometer with  $\text{CDCl}_3$  or  $\text{DMSO}-d_6$  as a solvent using  $\text{Me}_4\text{Si}$  as an internal standard. EI-Mass spectra were obtained on a JEOL JMS-Q1050GC Ultra Quad GC/MS spectrometer. The final products are stable in ambient conditions. Density functional theory (DFT) calculations were performed with Gaussian09 program (revision E.01) at the B3LYP/6-31G(d,p) level of theory for a full geometry optimization.<sup>S1</sup>

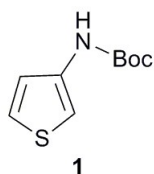
## II. Syntheses



**Scheme S1** Chemical structures of thienoisindigo (**TIIG**), diphenylthienoisindigo (**dph-TIIG**) and *N,N*-dihexyldiphenylthienoisindigo (*N*-hexyl **dph-TIIG**).

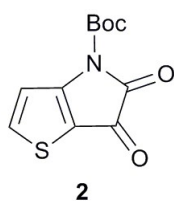
**TIIG** and **dph-TIIG** are new compounds. For comparison, *N*-hexyl **dph-TIIG** is prepared from the already reported compound, *N*-hexyl **TIIG**.<sup>S2</sup> Although *N*-(2-ethylhexyl) **dph-TIIG** has been reported previously,<sup>S3</sup> the alkyl chain is replaced by a hexyl chain.

### *tert*-Butyl thiophen-3-ylcarbamate (**1**)



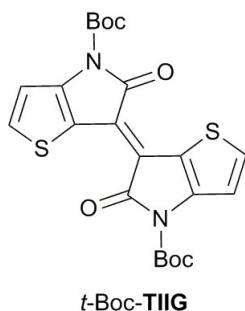
3-Thiophenecarboxylic acid (3.00 g, 23.4 mmol) was dissolved in *tert*-butyl alcohol (60 mL) under an argon atmosphere. To the resulting solution, diphenylphosphoryl azide (DPPA: 8.43 g, 30.6 mmol) and triethylamine (4.79 g, 47.3 mmol) were added successively, and the mixture was stirred at 80°C for 15 h. After the mixture was allowed to cool to room temperature, the solvent was evaporated under reduced pressure, and the residue was extracted with ethyl acetate and washed with saturated Na<sub>2</sub>CO<sub>3</sub> and brine. The organic layer was dried over MgSO<sub>4</sub>, and the solvent was removed under reduced pressure. The residue was purified by silica-gel chromatography eluted with hexane-ethyl acetate (4/1 = v/v) to afford **1** (3.24 g, 16.3 mmol, yield 70%) as a white solid. EI-MS *m/z*: 199 [*M*]<sup>+</sup>, 99 [*M* - CO<sub>2</sub> - C<sub>4</sub>H<sub>8</sub>]<sup>+</sup>. <sup>1</sup>H NMR (300 MHz, DMSO, 25°C): δ 9.58 (br s, 1H), 7.37 (dd, *J* = 5.1 Hz, 2.9 Hz, 1H), 7.16 (br s, 1H), 6.99 (dd, *J* = 5.1 Hz, 1.1 Hz, 1H), 1.46 (s, 9H). <sup>13</sup>C NMR (75 MHz, DMSO, 25°C): δ 152.69, 137.29, 124.49, 121.07, 105.72, 78.88, 28.05.

***tert*-Butyl 5,6-dioxo-5,6-dihydro-4*H*-thieno[3,2-*b*]pyrrole-4-carboxylate (**2**)**



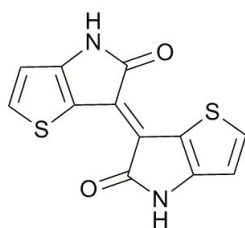
A solution of oxalyl chloride (1.24 g, 9.77 mmol) in anhydrous dichloromethane (20 mL) was cooled to 0°C under an argon atmosphere. A solution of **1** (1.50 g, 7.54 mmol) dissolved in anhydrous dichloromethane (30 mL) was dropwise added over 30 min. After 30 min, triethylamine (1.68 g, 16.6 mmol) was dropwise added over 3 h. The resulting mixture was allowed to warm to room temperature. After stirring for 12 h at room temperature, the mixture was quenched with water, and the organic layer was extracted with dichloromethane and washed with brine and water. The organic layer was dried over MgSO<sub>4</sub>, and the solvent was removed under reduced pressure. The residue was purified by silica-gel chromatography eluted with dichloromethane to afford **2** (0.89 g, 3.5 mmol, yield 46%) as a yellow solid. EI-MS *m/z*: 253 [*M*]<sup>+</sup>, 153 [*M* – CO<sub>2</sub> – C<sub>4</sub>H<sub>8</sub>]<sup>+</sup>, 152 [*M* – *t*-Boc]<sup>+</sup>. <sup>1</sup>H NMR (300 MHz, DMSO, 25°C): δ 8.49 (d, *J* = 5.1 Hz, 1H), 7.42 (d, *J* = 5.1 Hz, 1H), 1.56 (s, 9H). <sup>13</sup>C NMR (75 MHz, DMSO, 25°C): δ 170.19, 159.45, 158.29, 146.39, 144.14, 118.39, 115.81, 84.16, 27.58.

**Di-*tert*-butyl (E)-5,5'-dioxo-[6,6'-bithieno[3,2-*b*]pyrrolylidene]-4,4'(5*H*,5'*H*)-dicarboxylate (*t*-Boc-TIIG)**



Compound **2** (1.26 g, 4.98 mmol) and Lawesson's Reagent (1.01 g, 2.50 mmol) were dissolved in anhydrous toluene (50 mL) under an argon atmosphere. The resulting mixture was heated to 60°C and stirred for 12 h. After cooling to room temperature, the solvent was removed under reduced pressure. The residue was purified by silica-gel chromatography eluted with dichloromethane to afford *t*-Boc-TIIG (0.82 g, 1.73 mmol, yield 69%) as a red brown solid. EI-MS *m/z*: 474 [*M*]<sup>+</sup>, 374 [*M* – CO<sub>2</sub> – C<sub>4</sub>H<sub>8</sub>]<sup>+</sup>, 274 [*M* – 2 CO<sub>2</sub> – 2 C<sub>4</sub>H<sub>8</sub>]<sup>+</sup>. <sup>1</sup>H NMR (300 MHz, DMSO, 25°C): δ 7.93 (d, *J* = 5.1 Hz, 2H), 7.35 (d, *J* = 5.1 Hz, 2H), 1.61 (s, 9H).

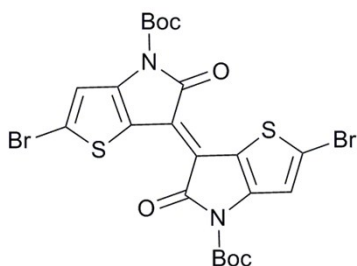
**(E)-[6,6'-Bithieno[3,2-b]pyrrolylidene]-5,5'(4H,4'H)-dione (TIIG)**



**TIIG**

A solution of *t*-Boc-TIIG (0.20 g, 0.42 mmol) in 2,2,2-trifluoroacetic acid (20 mL) was stirred for 1 h under an argon atmosphere. The suspension was filtered to afford TIIG (0.11 g, 0.40 mmol, yield 95%) as a purple brown solid. EI-MS  $m/z$ : 274  $[M]^+$ .  $^1\text{H}$  NMR (300 MHz, DMSO, 25°C):  $\delta$  10.87 (br s, 2H), 7.76 (d,  $J = 5.1$  Hz, 2H), 6.89 (d,  $J = 5.1$  Hz, 2H).  $^{13}\text{C}$  NMR (75 MHz, DMSO, 80°C):  $\delta$  172.19, 149.68, 134.86, 119.96, 113.85, 112.31. Anal. Calcd for  $\text{C}_{12}\text{H}_6\text{N}_2\text{O}_2\text{S}_2$ : C, 52.54; H, 2.20; N, 10.21; O, 11.66; S, 23.37; found: C, 52.55; H, 2.18; N, 10.12; O, 11.92; S, 23.40.

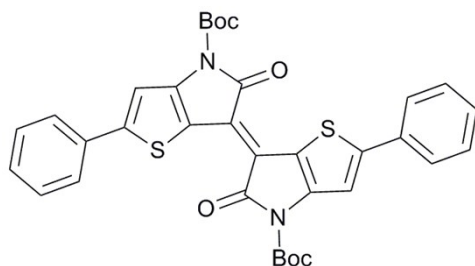
**Di-tert-butyl (E)-2,2'-dibromo-5,5'-dioxo-[6,6'-bithieno[3,2-b]pyrrolylidene]-4,4'(5H,5'H)-dicarboxylate (3)**



**3**

To a solution of *t*-Boc-TIIG (0.75 g, 1.58 mmol) dissolved in anhydrous dichloromethane (70 mL), *N*-bromosuccinimide (NBS: 0.65 g, 3.65 mmol) was added at room temperature, and the mixture was stirred under an argon atmosphere for 5 h. After the solvent was removed under reduced pressure, the residue was filtered with methanol to afford **3** (0.85 g, 1.34 mmol, yield 85%) as a brown solid. EI-MS  $m/z$ : 432  $[M - 2 \text{CO}_2 - 2 \text{C}_4\text{H}_8]^+$ .  $^1\text{H}$  NMR (300 MHz,  $\text{CDCl}_3$ , 25°C):  $\delta$  7.42 (s, 2H), 1.66 (s, 18H).

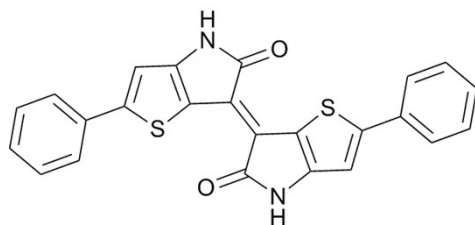
**Di-tert-butyl (*E*)-5,5'-dioxo-2,2'-diphenyl-[6,6'-bithieno[3,2-b]pyrrolylidene]-4,4'(5H,5'H)-dicarboxylate (*t*-Boc-dph-TIIG)**



***t*-Boc-dph-TIIG**

Compound **3** (0.40 g, 0.63 mmol) and Pd(PPh<sub>3</sub>)<sub>4</sub> (37 mg, 0.032 mmol) were dissolved in toluene (40 mL) under an argon atmosphere. To the resulting solution, trimethyl(phenyl)tin (0.46 g, 1.91 mmol) was added, and the mixture was stirred at 110°C for 24 h. After the mixture was allowed to cool to room temperature, methanol was added, and the solvent was evaporated under reduced pressure. The residue was purified by silica-gel chromatography eluted with dichloromethane to afford *t*-Boc-dph-TIIG (0.23 g, 0.37 mmol, yield 59%) as a purple blue solid. EI-MS *m/z*: 426 [*M* - 2 CO<sub>2</sub> - 2 C<sub>4</sub>H<sub>8</sub>]<sup>+</sup>. <sup>1</sup>H NMR (300 MHz, CDCl<sub>3</sub>, 25°C): δ 7.74 (d, *J* = 7.0 Hz, 4H), 7.65 (s, 2H), 7.46–7.37 (m, 6H), 1.72 (s, 18H).

**(*E*)-2,2'-Diphenyl-[6,6'-bithieno[3,2-b]pyrrolylidene]-5,5'(4H,4'H)-dione (dph-TIIG)**



**dph-TIIG**

**Dph-TIIG** was synthesized from *t*-Boc-dph-TIIG (0.022 g, 0.035 mmol) similarly to **TIIG**. **Dph-TIIG** (0.014 g, 0.033 mmol, yield 94%) was obtained as a blue black solid. EI-MS *m/z*: 426 [*M*]<sup>+</sup>. <sup>1</sup>H NMR (300 MHz, DMSO, 80°C): δ 10.93 (br s, 2H), 7.77 (d, *J* = 6.6 Hz, 4H), 7.48–7.37 (m, 6H), 7.29 (s, 2H). <sup>13</sup>C NMR (75 MHz, DMSO, 80°C): δ 171.82, 150.87, 150.18, 133.61, 128.79, 128.22, 125.12, 119.06, 113.87, 108.74. Anal. Calcd for C<sub>24</sub>H<sub>14</sub>N<sub>2</sub>O<sub>2</sub>S<sub>2</sub>: C, 67.59; H, 3.31; N, 6.57; O, 7.50; S, 15.03; found: C, 67.71; H, 3.41; N, 6.52; O, 7.60; S, 14.78.

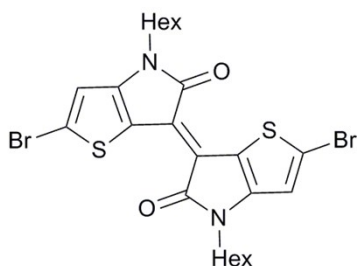
**(E)-4,4'-Dihexyl-[6,6'-bithieno[3,2-b]pyrrolylidene]-5,5'(4H,4'H)-dione (N-hexyl TIIG)**



**N-hexyl TIIG**

*N*-Hexyl **TIIG** was prepared according to the previous report.<sup>S2</sup>

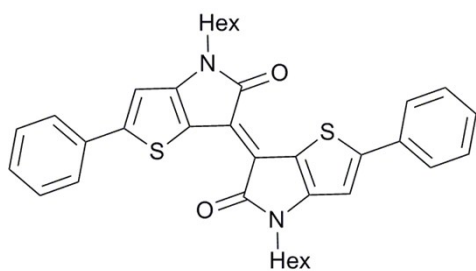
**(E)-2,2'-Dibromo-4,4'-dihexyl-[6,6'-bithieno[3,2-b]pyrrolylidene]-5,5'(4H,4'H)-dione (N-hexyl dBr-TIIG)**



**N-hexyl dBr-TIIG**

*N*-Hexyl **dBr-TIIG** was synthesized from *N*-hexyl **TIIG** (0.30 g, 0.68 mmol) and **NBS** (0.26 g, 1.46 mmol) similarly to **3**. The residue was purified by silica-gel chromatography eluted with hexane-dichloromethane (3/2 = v/v) to afford *N*-hexyl **dBr-TIIG** (0.29 g, 0.48 mmol, yield 71%) as a purple black solid. EI-MS  $m/z$ : 600 [ $M$ ]<sup>+</sup>. <sup>1</sup>H NMR (300 MHz, CDCl<sub>3</sub>, 25°C):  $\delta$  6.85 (s, 2H), 3.74 (t,  $J$  = 7.1 Hz, 4H), 1.73–1.64 (m, 4H), 1.40–1.26 (br m, 12H), 0.89 (t,  $J$  = 6.6 Hz, 6H). <sup>13</sup>C NMR (75 MHz, CDCl<sub>3</sub>, 25°C):  $\delta$  170.13, 149.90, 123.26, 119.81, 114.85, 114.71, 41.88, 31.39, 28.53, 26.52, 22.50, 13.97.

**(E)-4,4'-Dihexyl-2,2'-diphenyl-[6,6'-bithieno[3,2-b]pyrrolylidene]-5,5'(4H,4'H)-dione (N-hexyl dph-TIIG)**



**N-hexyl dph-TIIG**

*N*-Hexyl **dph-TIIG** was prepared from *N*-hexyl **dBr-TIIG** (0.30 g, 0.50 mmol), Pd(PPh<sub>3</sub>)<sub>4</sub> (29 mg, 0.025 mmol) and trimethyl(phenyl)tin (0.48 g, 1.99 mmol) similarly to *t*-Boc-**dph-TIIG**. *N*-hexyl **dph-TIIG** (0.17 g, 0.29 mmol, yield 58%) was obtained as a purple blue solid.

EI-MS *m/z*: 594 [*M*]<sup>+</sup>. <sup>1</sup>H NMR (300 MHz, CDCl<sub>3</sub>, 25°C): δ 7.73 (d, *J* = 7.0 Hz, 4H), 7.43–7.31 (m, 6H), 7.04 (s, 2H), 3.83 (t, *J* = 7.3 Hz, 4H), 1.81–1.72 (m, 4H), 1.43–1.28 (br m, 12H), 0.88 (t, *J* = 6.9 Hz, 6H). <sup>13</sup>C NMR (75 MHz, CDCl<sub>3</sub>, 25°C): δ 170.82, 152.53, 151.57, 134.35, 129.05, 128.59, 125.74, 120.10, 114.19, 107.20, 41.79, 31.48, 28.68, 26.62, 22.54, 14.00. Anal. Calcd for C<sub>36</sub>H<sub>38</sub>N<sub>2</sub>O<sub>2</sub>S<sub>2</sub>: C, 72.69; H, 6.44; N, 4.71; O, 5.38; found: C, 72.84; H, 6.52; N, 4.71; O, 5.76.

### III. Electrochemical properties, optical properties and DFT calculations

Cyclic voltammetry (CV) was carried out using an ALS model 701E electrochemical analyzer. The measurement was performed in a dehydrated DMF solution containing 0.1 M tetra-*n*-butylammonium hexafluorophosphate (*n*-Bu<sub>4</sub>N<sup>+</sup>PF<sub>6</sub><sup>-</sup>) as a supporting electrolyte using a glassy carbon working electrode, a platinum counter electrode, and an Ag/AgNO<sub>3</sub> electrode as a reference electrode at the scan rate of 50 mV s<sup>-1</sup>. The half-wave potential of ferrocene appeared at 0.05 V from the Ag/AgNO<sub>3</sub> reference electrode. From the first onset oxidation potential of **TIIG** and from the half-wave oxidation potential of **dph-TIIG** (Fig. S1), HOMO levels were estimated by assuming the ferrocene/ferrocenium energy level to be -4.8 eV under the vacuum level (Table S1).<sup>S4</sup> Since *N*-hexyl **dph-TIIG** displayed an irreversible oxidative peak at an onset potential of  $E_{\text{onset}} = 0.29$  V (Fig. S1), the HOMO level was determined to be -5.09 eV from this value. All compounds except for ferrocene did not show any noticeable peaks in the negative scan region.

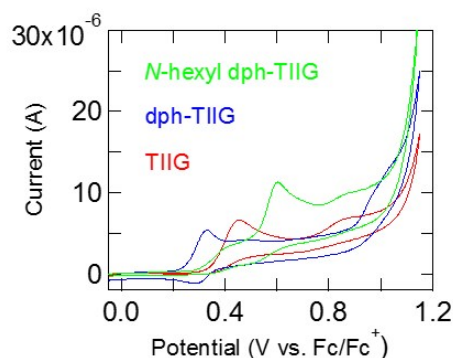


**Fig. S1** Cyclic voltammograms of **TIIG**, **dph-TIIG** and *N*-hexyl **dph-TIIG**.

UV-Vis spectra were measured on a Shimadzu Corporation UV-1800 in DMF solutions (Fig. S2). The optical gap of *N*-hexyl **dph-TIIG** is estimated to be 1.71 eV from the absorption edge of  $\lambda_{\text{onset}} = 725$  nm in a solution. The LUMO levels were estimated from the HOMO values and the optical gaps (Table S1). In comparison with the solution spectra, the absorption bands of thin films are shifted to long wavelengths because of the intermolecular interactions in the solid state. The results of the DFT calculations were depicted in Fig. S3.

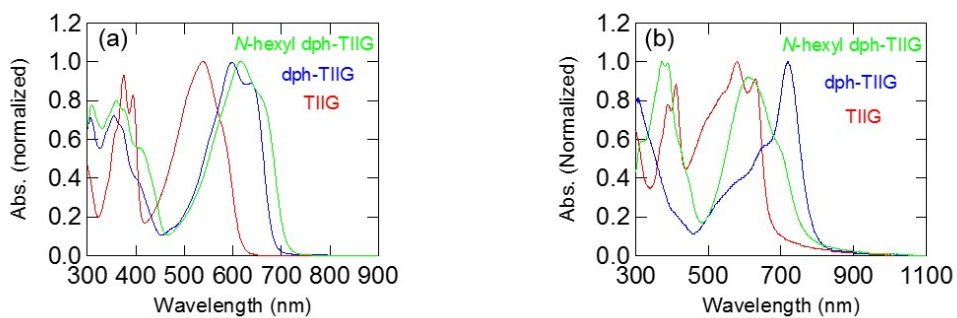


**Fig. S2** UV-vis absorption spectra of **TIIG**, **dph-TIIG** and **N-hexyl dph-TIIG** in (a) DMF solutions and for (b) thin films with the thickness of 20 nm thermally deposited on glass substrates.

**Table S1** Summary of electrochemical and optical properties.

	$E_{\text{HOMO}}$ (eV)	$E_{\text{LUMO}}$ (eV) <sup>a</sup>	$\lambda_{\text{max}}^{\text{sol}}$ (nm)	$\lambda_{\text{max}}^{\text{film}}$ (nm)	$E_{\text{g}}^{\text{opt}}$ (eV) <sup>b</sup>
<b>TIIG</b>	-5.14	-3.14	375, 394, 539	388, 410, 578, 630	2.00
<b>dph-TIIG</b>	-5.11	-3.32	306, 355, 598, 637	307, 719	1.79
<i>N</i> -hexyl <b>dph-TIIG</b>	-5.09	-3.38	309, 360, 616	316, 371, 614	1.71

<sup>a</sup> Estimated from the HOMO level of the oxidation step and the optical gap. <sup>b</sup> Estimated from the solution absorption edge.

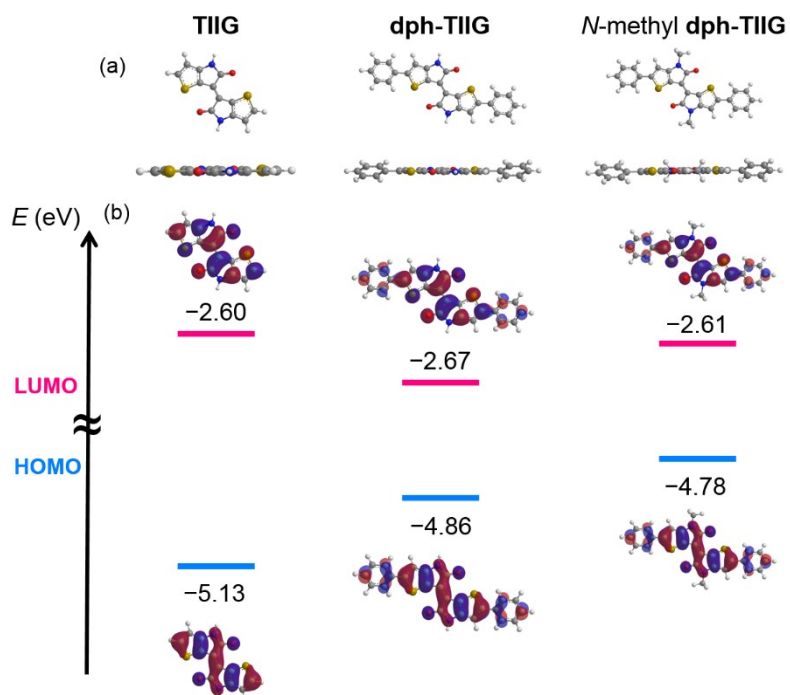


**Fig. S3** (a) Optimized molecular geometries and (b) the HOMO and LUMO levels together with the electron density distribution maps of the HOMO and LUMO levels in the neutral **TIIG** derivatives, estimated from the DFT calculations. In the third item, methyl groups were attached to the *N*-positions instead of hexyl groups for the DFT calculations.

#### IV. Thermal properties

Thermal gravimetric analyses (TGA) were performed using a RIGAKU Thermo plus EVO TG8120 thermal analyzer at the heating rate of  $10^{\circ}\text{C min}^{-1}$  under a nitrogen atmosphere (Fig. S4). Decomposition points were estimated from the temperatures of 5% weight loss to be **TIIG**:  $384.6^{\circ}\text{C}$ , **dph-TIIG**:  $444.1^{\circ}\text{C}$  and *N*-hexyl **dph-TIIG**:  $373.1^{\circ}\text{C}$ .

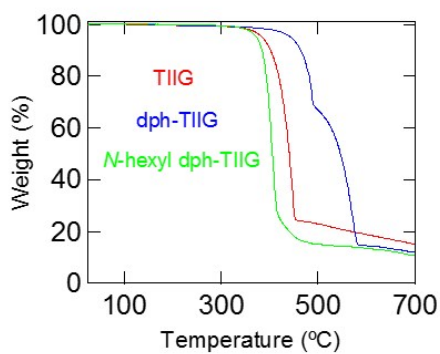


**Fig. S4** TGA curves of **TIIG**, **dph-TIIG** and *N*-hexyl **dph-TIIG**.

## V. Single crystal X-ray structure analyses and transfer integrals

Single-crystal X-ray structure analyses were carried out by a RIGAKU R-AXIS RAPID II imaging plate with Cu-K $\alpha$  radiation from a rotation anode source with a confocal multilayer X-ray mirror (RIGAKU VM-spider,  $\lambda = 1.54187 \text{ \AA}$ ). The crystal data were summarized in Table S2. The measurements were carried out at 171 K for **TIIG** and *N*-hexyl **dph-TIIG**, and 275 K for **dph-TIIG**. The structures were solved by the direct method (SIR 2008),<sup>S5</sup> and refined by the full-matrix least-squares method by applying anisotropic temperature factors for all non-hydrogen atoms using the SHELX-97 programs.<sup>S6</sup> The hydrogen atoms were placed at the geometrically calculated positions. The molecular packings of **TIIG** and **dph-TIIG** were depicted in Figs. S5 and S6. In order to analyze the intermolecular interactions, the intermolecular overlap integrals of HOMO and LUMO ( $S_i$ ) are estimated on the basis of the MOPAC, AM1 molecular orbital calculation.<sup>S7-S9</sup> The intermolecular transfer integrals  $t_i$  between HOMOs and LUMOs were calculated from the intermolecular overlap integrals,  $S_i$  as  $t_i = E \times S_i$  by assuming the energy level  $E$  to be  $-10 \text{ eV}$  (Table S3).

**Table S2** Crystallographic data.

	<b>TIIG</b>	<b>dph-TIIG</b>	<i>N</i> -hexyl <b>dph-TIIG</b>
Chemical formula	C <sub>12</sub> H <sub>6</sub> N <sub>2</sub> O <sub>2</sub> S <sub>2</sub>	C <sub>24</sub> H <sub>14</sub> N <sub>2</sub> O <sub>2</sub> S <sub>2</sub>	C <sub>36</sub> H <sub>38</sub> N <sub>2</sub> O <sub>2</sub> S <sub>2</sub>
Formula weight	274.31	426.51	594.83
Crystal shape	brown plate	black plate	black plate
Crystal system	monoclinic	orthorhombic	triclinic
Space group	<i>P2</i> <sub>1</sub> / <i>n</i>	<i>Pbca</i>	<i>P</i> -1
<i>a</i> (Å)	8.23564(15)	7.88168(10)	4.99713(13)
<i>b</i> (Å)	4.76654(9)	7.13603(10)	10.7672(3)
<i>c</i> (Å)	14.1245(3)	35.6666(9)	14.6977(4)
$\alpha$ (°)	90	90	102.0088(17)
$\beta$ (°)	96.7481(7)	90	92.7147(16)
$\gamma$ (°)	90	90	101.1171(16)
<i>V</i> (Å <sup>3</sup> )	550.63(2)	2006.03(6)	755.83(4)
<i>Z</i>	2	4	1
Unique refls. ( $R_{\text{int}}$ )	1009 (0.0398)	1835 (0.0911)	2694 (0.0712)
$D_{\text{calc}}$ (g/cm <sup>3</sup> )	1.654	1.412	1.307
$R_1^{\text{a}}$	0.0347	0.0651	0.0714
$R_w^{\text{b}}$	0.0906	0.1838	0.2364
GOF	1.118	1.023	1.052

$$^{\text{a}} R_1 = \frac{\sum |F_o| - |F_c|}{\sum |F_o|} \cdot \quad ^{\text{b}} R_w = \left[ \frac{\sum w(F_o - |F_c|)^2}{\sum wF_o^2} \right]^{1/2}$$

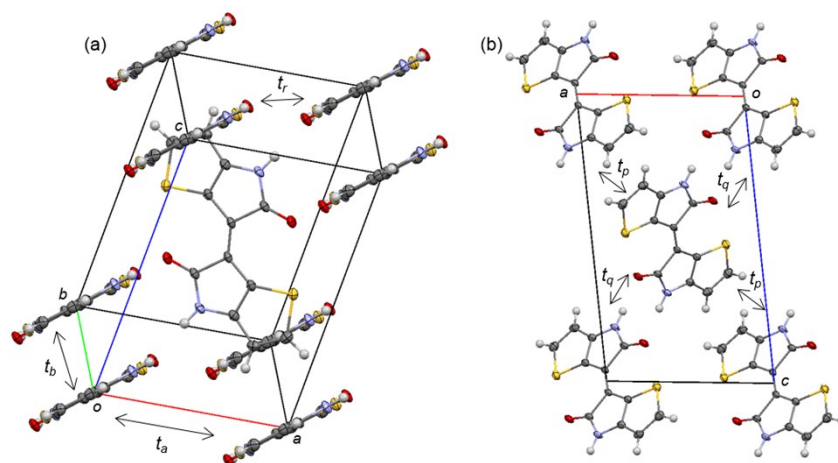


**Fig. S5** Crystal structure of TIIG: (a) the molecular packing and (b) crystal structure viewed along the  $b$  axis.

**Table S3** Transfer integrals of TIIG.

$t$ (meV)	$t_a$	$t_b$	$t_r$	$t_p$	$t_q$
HOMO	-0.17	7.69	-0.12	2.52	0.06
LUMO	0.25	57.3	-0.09	1.70	0.08

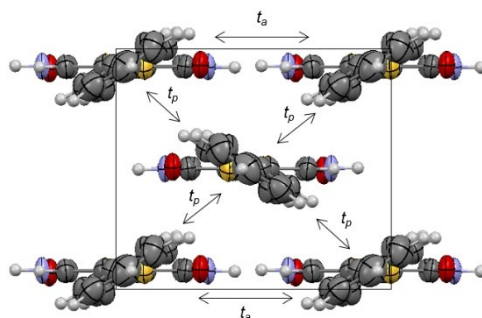


**Fig. S6** Crystal structure of **dph-TIIG** viewed along the molecular long axis. The transfer integrals for HOMO/LUMO are  $t_a$ : 0.21/0.68 and  $t_p$ : -11.2/-6.06 meV.

For comparison, plate-like single crystals of *N*-hexyl **dph-TIIG** were obtained by sublimation and the X-ray single-crystal structure analysis was carried out (Fig. S7). *N*-hexyl **dph-TIIG** has a uniform stacking structure along the  $a$  axis with the interplanar spacing of 3.40 Å, and the alkyl chains are closely packed extending along the  $c$  axis due to the so called molecular fastener effect of the alkyl chains. The intramolecular S $\cdots$ O interaction is 2.86 Å, and *N*-hexyl **dph-TIIG** does not have any short S $\cdots$ S contact. In contrast to **dph-TIIG**, phenyl groups and central **TIIG** part are almost coplanar (dihedral angle is 0.8°) because molecular fastener effect of the alkyl chains affects molecular packing and conformation although thermodynamically most stable conformation is phenyl rings-tilted conformation like **dph-TIIG** as seen in the DFT calculations. It is expected from the crystal structures that *N*-hexyl **dph-TIIG** constructs a

one-dimensional conduction path, whereas *N*-unsubstituted **dph-TIIG** forms a two-dimensional conduction path.

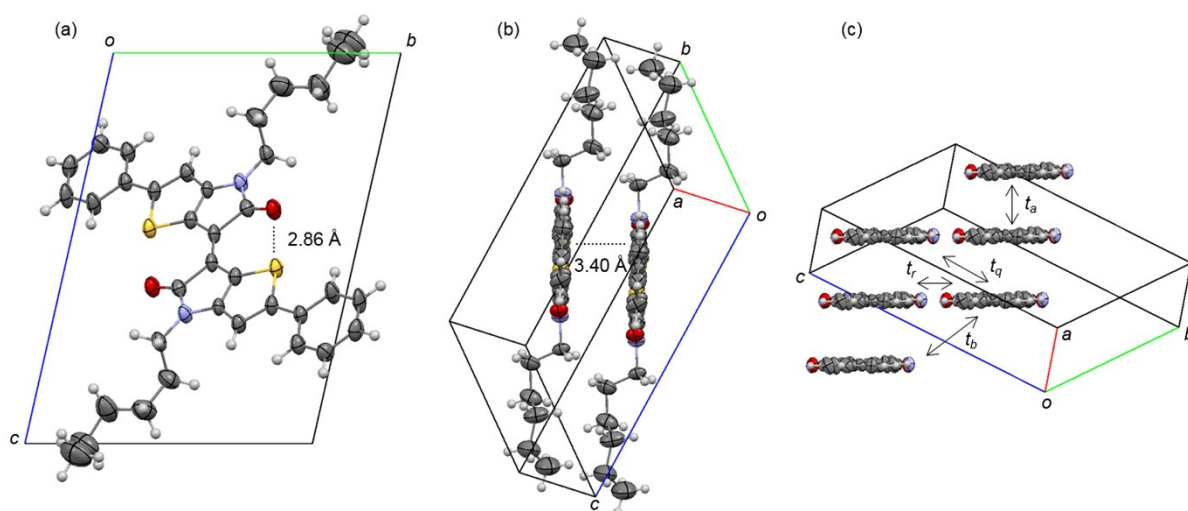


**Fig. S7** Crystal structure of *N*-hexyl **dph-TIIG**: (a) crystal structure viewed along the *a* axis and (b) the molecular packing. (c) Viewed from the molecular long axis, in which the alkyl chains are omitted for clarity. The transfer integrals for HOMO/LUMO are  $t_a$ : 29.6/61.6,  $t_b$ : -1.31/-0.05,  $t_q$ : -0.09/-0.01 and  $t_r$ : 0.07/0.53 meV.

## VI. Transistor fabrication and thin-film transistor properties

Thin-film transistors were fabricated onto n-doped Si substrates with a thermally grown SiO<sub>2</sub> dielectric layer (300 nm,  $C = 11.5 \text{ nF/cm}^2$ ). For the thin-film device, the passivation layer tetratetracontane (C<sub>44</sub>H<sub>90</sub>, TTC,  $\epsilon = 2.5$ ) was evaporated under a vacuum of  $10^{-3} \text{ Pa}$  on the substrates with a thickness of 20 nm,<sup>S10,S11</sup> where the resulting overall capacitance of the gate dielectrics was  $10.4 \text{ nF/cm}^2$ .<sup>S12</sup> Then the active layer was formed by thermal deposition under a vacuum of  $10^{-3} \text{ Pa}$ , in which the resulting thickness was 50 nm. The top-contact electrodes were patterned by thermal deposition of Au using a shadow mask; the channel length ( $L$ ) and width ( $W$ ) were 100  $\mu\text{m}$  and 1000  $\mu\text{m}$ , respectively. The organic field-effect transistor (OFET) properties were measured under the vacuum of  $10^{-3} \text{ Pa}$  by using a Keithley 4200 semiconductor parameter analyzer. The field-effect mobility ( $\mu$ ) and threshold voltage ( $V_T$ ) were calculated in the saturation regime by using the equation,  $I_{DS} = \mu(WC_i/2L)(V_G - V_T)^2$ , where  $I_{DS}$  and  $V_G$  are the drain current and gate voltage, respectively. Then,  $\mu$  was extracted from the slope where the  $\sqrt{I_{DS}}$  vs.  $V_G$  plot was straight.

*N*-hexyl **dph-TIIG** showed ambipolar transistor characteristics (Fig. S8), and mobilities decrease approximately two orders compared with **dph-TIIG**. OFET properties of all **TIIG** derivatives were summarized in Table S4.

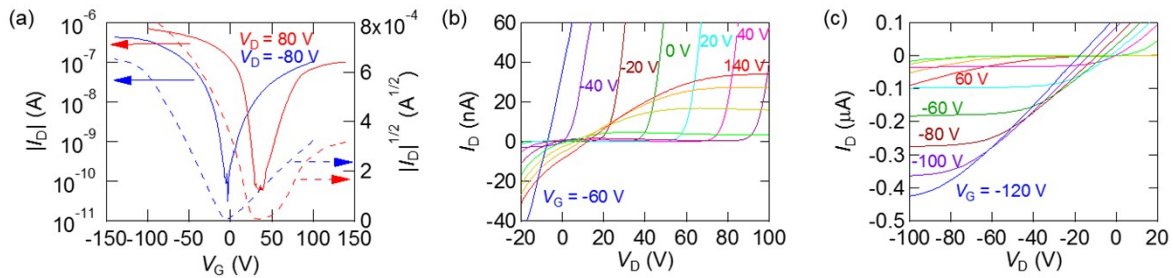


**Fig. S8** (a) Transfer, (b) n-channel, and (c) p-channel output characteristics based on *N*-hexyl **dph-TIIG**. Gate voltages ( $V_G$ ) are changed from  $-60 \text{ V}$  to  $140 \text{ V}$  for n-channel scan and from  $60 \text{ V}$  to  $-120 \text{ V}$  for p-channel scan with  $20 \text{ V}$  steps.

**Table S4** Summary of OFET properties.

Compound	electron		hole			
	$\mu_{\text{avg}} (\mu_{\text{max}})$ ( $\text{cm}^2 \text{V}^{-1} \text{s}^{-1}$ )	$V_T$ (V)	$I_{\text{on}}/I_{\text{off}}$	$\mu_{\text{avg}} (\mu_{\text{max}})$ ( $\text{cm}^2 \text{V}^{-1} \text{s}^{-1}$ )	$V_T$ (V)	$I_{\text{on}}/I_{\text{off}}$
<b>TIIG</b>	$2.5 \times 10^{-3}$ ( $2.9 \times 10^{-3}$ )	55.8	$10^6$	$1.3 \times 10^{-3}$ ( $1.6 \times 10^{-3}$ )	-62.4	$10^4$
<b>dph-TIIG</b>	0.102 (0.13)	77.1	$10^5$	0.084 (0.12)	-13.9	$10^6$
<i>N</i> -hexyl	$6.4 \times 10^{-4}$	58.7	$10^3$	$1.1 \times 10^{-3}$	-4.3	$10^4$
<b>dph-TIIG</b>	( $7.6 \times 10^{-4}$ )			( $1.5 \times 10^{-3}$ )		

## VII. Thin film microstructures and morphologies

Atomic force microscopy (AFM) images were taken by an SII scanning probe microscope system SPI3800N and SPA-300 by using an  $\text{Si}_3\text{N}_4$  cantilever in air. The XRD patterns were taken by using a Philips X'Pert-Pro-MRD with  $\text{CuK}\alpha$  radiation ( $\lambda = 1.540598 \text{ \AA}$ ). Two-dimensional grazing incidence wide-angle X-ray scattering (GIWAXS) patterns were obtained at SPring-8 on beamline BL45XU.<sup>S13</sup> The samples were irradiated at a fixed incident angle on the order of  $0.10^\circ$  and the GIWAXS patterns were recorded with a 2-D image detector (PILATUS3X 2M). The wavelength of the X-ray beam was  $0.1 \text{ nm}$  (energy of  $12.39 \text{ KeV}$ ) and the camera length was  $263 \text{ mm}$  for **TIIG**,  $340 \text{ mm}$  for **dph-TIIG**, and  $341 \text{ mm}$  for *N*-hexyl **dph-TIIG**.

The thin film of **TIIG** shows small fibril-like grains disconnected with each other with definitive boundaries (Fig. S9 (a)). In contrast, **dph-TIIG** and *N*-hexyl **dph-TIIG** consist of densely packed relatively large fibril-like grains (Figs. S9 (b) and (c)). This difference is related to the mobilities.

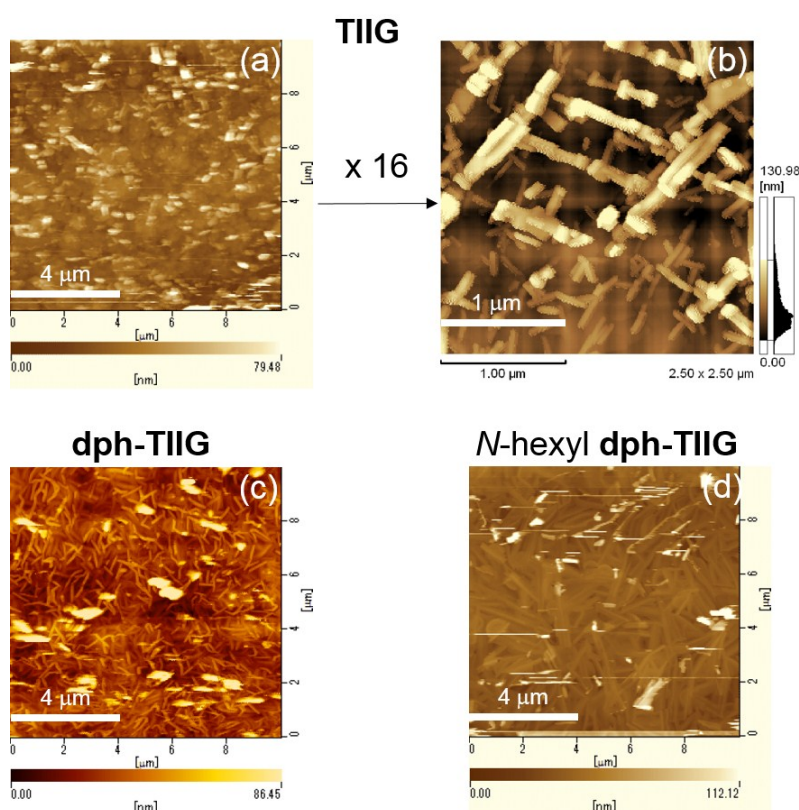


**Fig. S9** AFM images of (a) and (b) thin films of **TIIG**, (c) thin film of **dph-TIIG** and (d) thin film of *N*-hexyl **dph-TIIG**.

The XRD patterns are shown in Figs. S10 (a), S11 (a) and S12 (a). These XRD patterns show additional peaks attributable to the passivation layer (TTC). For **TIIG**, the  $d$ -spacing is estimated to be 7.4 Å (Fig. S10 (a)), which is very close to  $1/2 c \sin\beta$  (7.0 Å) of the crystal lattice. This value corresponds to  $q_z = 0.85 \text{ Å}^{-1}$  ( $= 7.39 \text{ Å}$ ) in the GIWAXS pattern (Fig. S10 (b)). The in-plane GIWAXS pattern shows a  $\pi$ - $\pi$  stacking peak at  $q_{xy} = 1.66 \text{ Å}^{-1}$  ( $= 3.79 \text{ Å}$ ) (Fig. S10 (b)). Another peak observed at  $q_{xy} = 1.51 \text{ Å}^{-1}$  ( $= 4.16 \text{ Å}$ ) is consistent with half of the crystallographic  $a$  axis (4.12 Å). These observations indicate that the crystallographic  $ab$  plane is aligned parallel to the substrate (Fig. S10 (c)). Therefore, the molecular tilt angle from the vertical direction to the substrate is  $25.1^\circ$ .

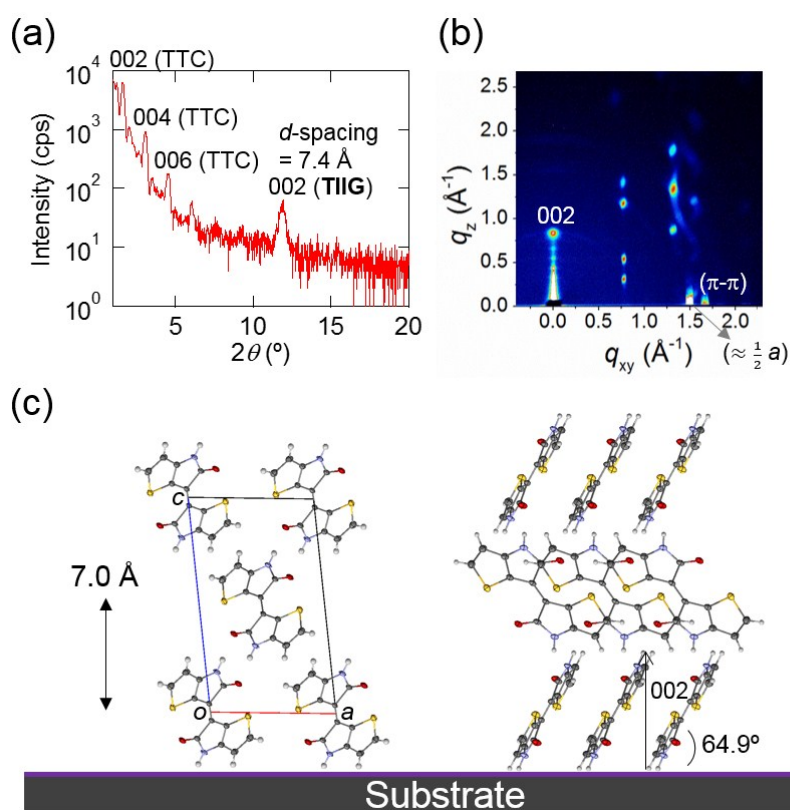


**Fig. S10** (a) X-ray diffraction pattern, (b) GIWAXS pattern of thin films of **TIIG** and (c) molecular arrangements on the substrate.

The XRD pattern of the **dph-TIIG** thin film shows the  $d$ -spacing of 18.8 Å (Fig. S11 (a)), corresponding to the interlayer direction. The GIWAXS pattern in Fig. S11 (b) shows a similar value of  $q_z = 0.33 \text{ Å}^{-1}$  ( $= 18.9 \text{ Å}$ ). The in-plane GIWAXS pattern shows a  $\pi$ - $\pi$  stacking distance of  $q_{xy} = 1.68 \text{ Å}^{-1}$  ( $= 3.74 \text{ Å}$ ). Another peak at  $q_{xy} = 1.52 \text{ Å}^{-1}$  ( $= 4.15 \text{ Å}$ ) is very close to half of the crystallographic  $a$  axis (3.94 Å), indicating that the  $a$  axis is parallel to the substrate. Then, the crystallographic  $ab$  plane is aligned parallel to the substrate, and the  $c$  axis is perpendicular to the substrate. However, the interlayer  $d$ -spacing (18.8 Å) is considerably larger than half of the crystallographic  $c$  axis (17.8 Å). This suggests the molecules in the thin films are less tilted than the molecules in the single crystals. The thin-film tilt angle ( $\beta'$ ) is calculated from  $l = d / \cos \beta'$ , where  $l$  is the molecule length estimated from the crystal structure (19.0 Å), and  $d$  is the  $d$ -spacing in the XRD pattern (18.8 Å). This leads to  $\beta' = 8.3^\circ$ , which is remarkably smaller than the single-crystal value,  $24^\circ$ . In the thin films, the molecules are packed more close to the perpendicular direction than the single crystals (Fig. S11 (c)).

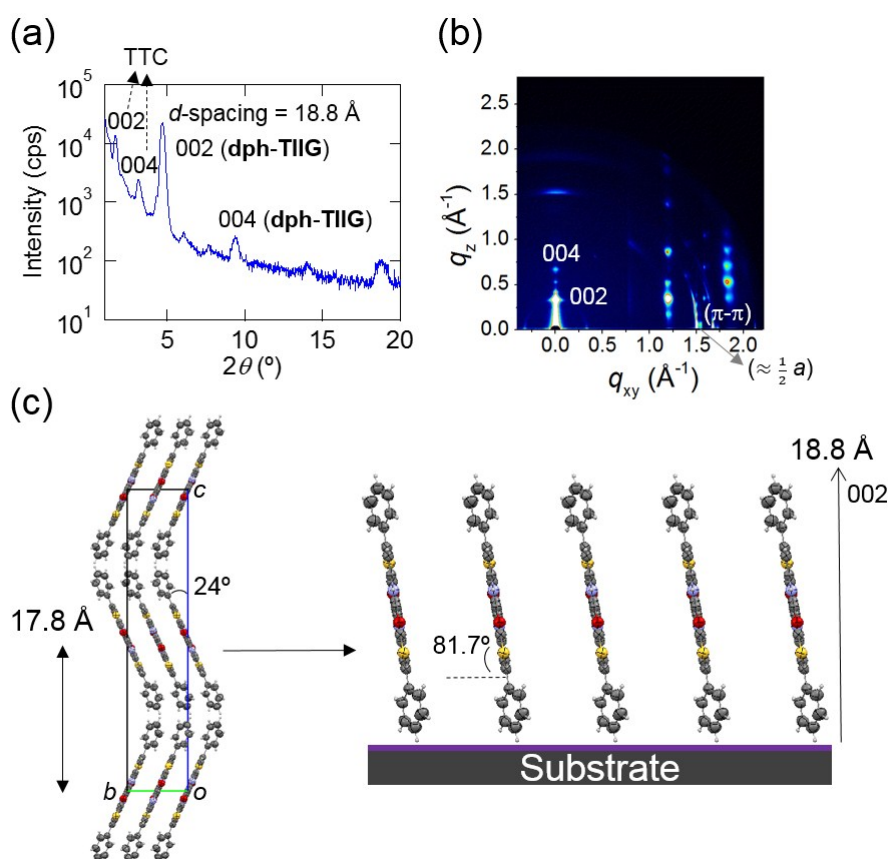


**Fig. S11** (a) X-ray diffraction pattern, (b) GIWAXS pattern of thin films of **dph-TIIG** and (c) molecular arrangements on the substrate.

From the XRD pattern of *N*-hexyl **dph-TIIG** thin films, the *d*-spacing is estimated to be 14.3 Å (Fig. S12 (a)). The GIWAXS pattern in Fig. S12 (b) shows the corresponding value,  $q_z = 0.44 \text{ \AA}^{-1}$  ( $= 14.3 \text{ \AA}$ ). This *d*-spacing ( $d = 14.3 \text{ \AA}$ ) corresponds to  $c \sin \alpha \sin \beta$  (14.4 Å), indicating that the crystallographic *ab* plane is aligned parallel to the substrate (Fig. S12(c)). Therefore, the molecular tilt angle from the vertical direction to the substrate is  $35.5^\circ$ . The  $\pi$ - $\pi$  stacking is estimated to be  $q_{xy} = 1.70 \text{ \AA}^{-1}$  ( $= 3.70 \text{ \AA}$ ).

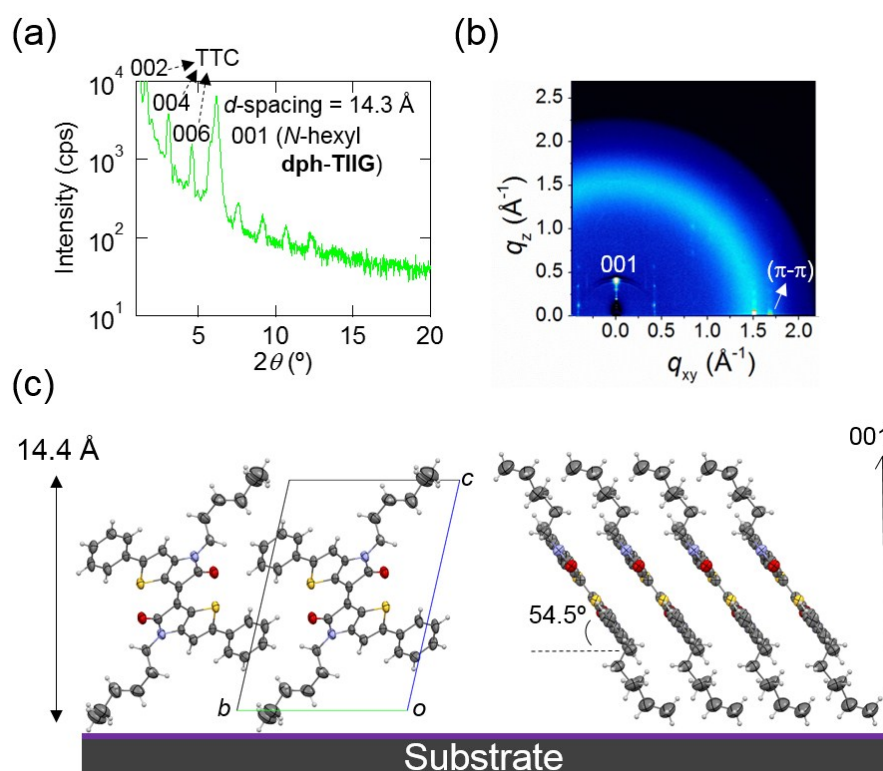


**Fig. S12** (a) X-ray diffraction pattern, (b) GIWAXS pattern of thin films of *N*-hexyl **dph-TIIG** and (c) molecular arrangements on the substrate.

## References

- S1 M. J. Frisch, G. W. Trucks, H. B. Schlegel, G. E. Scuseria, M. A. Robb, J. R. Cheeseman, G. Scalmani, V. Barone, B. Mennucci, G. A. Petersson, H. Nakatsuji, M. Caricato, X. Li, H. P. Hratchian, A. F. Izmaylov, J. Bloino, G. Zheng, J. L. Sonnenberg, M. Hada, M. Ehara, K. Toyota, R. Fukuda, J. Hasegawa, M. Ishida, T. Nakajima, Y. Honda, O. Kitao, H. Nakai, T. Vreven, J. A. Montgomery, Jr., J. E. Peralta, F. Ogliaro, M. Bearpark, J. J. Heyd, E. Brothers, K. N. Kudin, V. N. Staroverov, T. Keith, R. Kobayashi, J. Normand, K. Raghavachari, A. Rendell, J. C. Burant, S. S. Iyengar, J. Tomasi, M. Cossi, N. Rega, J. M. Millam, M. Klene, J. E. Knox, J. B. Cross, V. Bakken, C. Adamo, J. Jaramillo, R. Gomperts, R. E. Stratmann, O. Yazyev, A. J. Austin, R. Cammi, C. Pomelli, J. W. Ochterski, R. L. Martin, K. Morokuma, V. G. Zakrzewski, G. A. Voth, P. Salvador, J. J. Dannenberg, S. Dapprich, A. D. Daniels, O. Farkas, J. B. Foresman, J. V. Ortiz, J. Cioslowski and D. J. Fox, GAUSSIAN 09 (Revision E.01), Gaussian, Inc., Wallingford CT, 2013.
- S2 T. Hasegawa, M. Ashizawa and H. Matsumoto, *RSC Adv.*, 2015, **5**, 61035–61043.
- S3 H. Kang, S. Y. An, B. Walker, S. Song, T. Kim, J. Y. Kim and C. Yang, *J. Mater. Chem. A*, 2015, **3**, 9899–9908.
- S4 J. Pommerehne, H. Vestweber, W. Guss, R. F. Mahrt, H. Bäessler, M. Porsch and J. Daub, *Adv. Mater.*, 1995, **7**, 551–554.
- S5 M. C. Burla, R. Caliandro, M. Camalli, B. Carrozzini, G. L. Casciarano, L. De Caro, C. Giacovazzo, G. Polidori, D. Siliqi and R. Spagna, *J. Appl. Crystallogr.*, 2007, **40**, 609–613.
- S6 G. M. Sheldrick, *Acta Crystallogr. A.*, 2008, **64**, 112–122.
- S7 T. Mori, A. Kobayashi, Y. Sasaki, H. Kobayashi, G. Saito and H. Inokuchi, *Bull. Chem. Soc. Jpn.*, 1984, **57**, 627–633.
- S8 M. J. S. Dewar, E. G. Zoebisch, E. F. Healy and J. J. P. Stewart, *J. Am. Chem. Soc.*, 1985, **107**, 3902–3909.
- S9 M. J. S. Dewar and Y. C. Yuan, *Inorg. Chem.*, 1990, **29**, 3881–3890.
- S10 M. Kraus, S. Richler, A. Opitz, W. Brütting, S. Haas, T. Hasegawa, A. Hinderhofer and F. Schreiber, *J. Appl. Phys.*, 2010, **107**, 094503.
- S11 M. Kraus, S. Haug, W. Brütting and A. Opitz, *Org. Electron.*, 2011, **12**, 731–735.
- S12 K.-J. Baeg, Y.-Y. Noh, J. Ghim, B. Lim and D.-Y. Kim, *Adv. Funct. Mater.*, 2008, **18**, 3678–3685.
- S13 T. Fujisawa, K. Inoue, T. Oka, H. Iwamoto, T. Uruga, T. Kumasaka, Y. Inoko, N. Yagi, M. Yamamoto and T. Ueki, *J. Appl. Crystallogr.*, 2000, **33**, 797–800.